Glass-Forming Ability and Early Crystallization Kinetics of Novel Cu-Zr-Al-Co Bulk Metallic Glasses

Xiaoliang Han [1], Yusheng Qin [1], Kai Qin [2], Xuelian Li [1], Shenghai Wang [1], Jun Mi [1], Kaikai Song [1],* and Li Wang [1],*

[1] School of Mechanical, Electrical & Information Engineering, Shandong University (Weihai), Wenhua Xilu 180, Shandong 264209, China; hanxiaoliang92@163.com (X.H.); qinyusheng166@163.com (Y.Q.); hunterlxl@163.com (X.L.); shenghaiw@163.com (S.W.); mijunsdu@outlook.com (J.M.)

[2] Department of Physics, School of Science, Northwestern Polytechnical University, Youyi Xilu 127, Shanxi 710072, China; amazingqk@outlook.com

* Correspondence: songkaikai8297@gmail.com (K.S.); wanglihxf@sdu.edu.cn (L.W.); Tel.: +86-631-568-8224 (K.S. & L.W.)

Abstract: In recent years, CuZr-based bulk metallic glass (BMG) composites ductilized by a shape memory B2 CuZr phase have attracted great attention owing to their outstanding mechanical properties. However, the B2 CuZr phase for most CuZr-based glass-forming compositions is only stable at very high temperatures, leading to the uncontrollable formation of B2 crystals during quenching. In this work, by introducing Co (i.e., 4, 5, and 6 at. %) and 10 at. % Al into CuZr-based alloys, the relatively good glass-forming ability (GFA) of CuZr-based alloys still can be achieved. Meanwhile, the B2 phase can be successfully stabilized to lower temperatures than the final temperatures of crystallization upon heating CuZr-based BMGs. Unlike previous reported CuZr-based BMGs, the primary crystallization products upon heating are mainly B2 CuZr crystals but not $CuZr_2$ and $Cu_{10}Zr_7$ crystals. Furthermore, the primary precipitates during solidification are still dominated by B2 crystals, whose percolation threshold is detected to lie between 10 ± 2 vol. % and 31 ± 2 vol. %. The crystallization kinetics underlying the precipitation of B2 crystals was also investigated. Our results show that the present glass-forming composites are promising candidates for the fabrication of ductile CuZr-based BMG composites.

Keywords: metallic glasses; rapid solidification; glass-forming ability; crystallization

1. Introduction

Composites have been designed in an attempt to accomplish an optimal trade-off between strength and ductility in many classes of materials, which exhibit superior mechanical properties compared with either constituent material alone [1–3]. In the past decades, a new class of composites, called bulk metallic glass (BMG) composites, have been explored by introducing ductile crystalline phases ex situ or in situ in a glassy matrix in order to enhance the ductility or/and toughness at the cost of the high strength of intrinsically brittle BMGs [4–15]. During deformation, ductile crystals in BMG composites may serve as heterogeneous nucleation sites for the initiation of shear bands and act as attraction or pinning centers during shear band propagation. This leads to the formation of multiple shear bands in the glassy matrix and then the enhancement of room-temperature ductility [16–19]. However, the strain softening induced by the formation of shear bands in the glassy matrix cannot be compensated by the strain hardening provided by these ductile phases during deformation. Overall, the microscopic strain-softening of BMG composites dominates their plastic deformation [4–19]. In this regard, shape memory B2 CuZr crystals were introduced into a glassy matrix as an alternative reinforcing phase because the B2 CuZr crystals usually show a pronounced work hardening during deformation due

to the unique transformation-mediated deformation mechanism [20–29]. As a result, such BMG composites show not only good tensile plastic deformation ability but also work-hardening capacity, which further promotes the development of BMGs to be used as structural materials in future [20–32]. Until now, many CuZr-based glass-forming compositions have explored to fabricate ductile BMG composites with obvious work hardening [20–32].

Usually, during rapid solidification, the formation of B2 CuZr crystals in the CuZr-based glassy matrix, including their distributions, volume fractions, and gran sizes, strongly depends on the cooling rates, casting temperatures, and melting frequency of master alloys. By carefully controlling the casting parameters mentioned above during solidification, BMG composites with good mechanical properties could be prepared [20–33]. However, the optimum microstructures of CuZr-based BMG composites processing homogenously distributed and appropriate volume fractions of relatively fine B2 crystals only can be simultaneously obtained by considering two key factors: (1) inhibiting the easy decomposition of the high-temperature metastable B2 CuZr phase into the low-temperature equilibrium phases (i.e., $CuZr_2$, $Cu_{10}Zr_7$ or other equilibrium crystals) via a eutectoid reaction during solidification by controlling compositions of CuZr-based alloys [20–32]; (2) avoiding the interpenetration of B2 spherical crystals during solidification when their volume fractions reach a critical crystalline volume fraction between 30 and 50 vol. % [29,30]. In other words, in order to control the formation of the B2 CuZr phase during quenching, it should be considered to stabilize the B2 CuZr phase with minor element additions instead of only adjusting the casting process. Both of these factors raise a big challenge to manipulate the formation of the B2 phase during rapid quenching so as to explore CuZr-based shape memory BMG composites with optimum mechanical properties.

Previous results have demonstrated that more than 4 at. % Co addition into near-equiatomic Cu-Zr binary alloys can significantly enhance the thermal stability of the B2 CuZr phase so that the B2 CuZr phase can be easily preserved at low temperatures [34–36]. However, the glass-forming ability (GFA) of CuZr-based alloys with the addition of Co can be gravely deteriorated, and only amorphous ribbons can be produced. Under these circumstances, other micro-alloying elements should be also introduced into CuZr-based alloys in an attempt to maintain the GFA or reduce the deterioration of GFA induced by the Co addition [34–36]. It has been found that the addition of Al, Ag, Ti, or rare earth metals can enhance the GFA of CuZr-based alloys even though the thermal stability of the B2 CuZr phase cannot be effectively improved at the same time [37–41]. Therefore, systematic investigations have been devoted to fabricate Cu-Zr-Al-Co BMGs and their composites by carefully adjusting the contents of Al and Co [31,42–44]. However, so far, a balance between the thermal stability of the B2 CuZr phase and the GFA of the CuZr-based alloy has not yet been achieved [31,42–44]. On the one other hand, another method, i.e., partially crystallizing a glass in an extremely short time, was proposed to fabricate ductile CuZr-based BMG composites [45,46]. However, the major crystallization products of CuZr-based BMGs during annealing are $Cu_{10}Zr_7$, and/or $CuZr_2$ and others, but not the B2 CuZr phase [33]. Meanwhile, the B2 CuZr phase only exists at higher temperatures than the final temperature of crystallization [33]. Hence, both the heating and cooling rates and the annealing temperature during partial crystallizing must be very high, which severely restricts the widespread use of this preparation method.

Therefore, it is desirable to explore new CuZr-based BMGs with good GFA, whose major crystallization products become the B2 CuZr phase, in order to easily fabricate CuZr-based BMG composites by controlling the rapid solidification of melts or fast and partial-crystallizing BMGs. In this paper, $(Cu_{0.5}Zr_{0.5})_{90-x}Al_{10}Co_x$ (x = 4, 5, and 6 at. %) BMGs with good GFA and high thermal stability were successfully prepared, and their major crystallization products are the B2 CuZr phase. Their crystallization kinetics were also investigated.

2. Materials and Methods

The $(Cu_{0.5}Zr_{0.5})_{90-x}Al_{10}Co_x$ (x = 4, 5, and 6 at. %) master alloys were prepared by arc melting appropriate amounts of the constituting elements (>99.9% purity) under a Ti-gettered argon

atmosphere, which were remelted at least for three times to achieve chemical homogeneity. Then master alloys were cast into rods with a diameter of 2 mm and a length of 55 ± 15 mm via a suction casting device (i.e., custom-made in Germany) under an argon atmosphere. An arc-melting current of 280 A for approximately 8 s was applied during suction casting. Furthermore, a wedge-shaped rod was also prepared by an injection machine (i.e., custom made in Germany) at an argon atmosphere, whose casting temperature was set to be 1473 ± 10 K. The phase analysis of the as-cast samples was characterized by the X-ray diffraction (XRD) in a transmission geometry (STOE STADI P, Dresden, Germany) or in a reflection mode (Rigaku D/max-rB, Weihai, China), respectively. The glass transition temperatures, T_g, the onset temperatures of crystallization, T_x, and the liquidus temperatures, T_L, of the as-cast rods were measured using a differential scanning calorimetry (DSC, Netzsch 404C, Jinan, China) under a flow of purified argon at a heating rate of 20 K/min. Additionally, the glass transition temperatures and the crystallization behaviors were also checked using a differential scanning calorimetry (DSC, Perkin-Elmer Diamond, Dresden, Germany) under a flow of high purity argon at heating rates of 5, 10, 20, and 40 K/min. The as-cast samples were first annealed at the temperatures between T_g and the finish temperature ($T_{\text{cryst-final}}$) of crystallization for $(Cu_{0.5}Zr_{0.5})_{90-x}Al_{10}Co_x$ (x = 4, 5, and 6 at. %) at a heating rate of 40 K/min and a cooling rate of 100 K/min, whose phases were also characterized by an XRD device. The morphology of the precipitates (i.e., sizes, distributions and volume fractions) in the annealed samples were observed using a scanning electron microscopes (SEM, Gemini 1530, Dresden, Germany) equipped with an energy-dispersive X-ray (EDX, Bruker AXS, Dresden, Germany) device.

3. Results and Discussion

3.1. Formation of Cu-Zr-Al-Co Bulk Metallic Glasses with Good Glass-Forming Ability

Previous reports have shown that with increasing Co from 0 at. % to 10 at. %, the GFA of CuZr-based alloys decreases dramatically [42–44]. However, the B2 CuZr phase can be effectively stabilized at room temperature when the content of Co exceeds 4 at. %, which causes the formation of only amorphous ribbons but not bulk amorphous samples. Lu et al. proposed a parameter, γ (=$T_x/(T_g + T_L)$), to evaluate the GFA [47] and found that, usually, the larger the γ is, the better the GFA the alloy has. It has been demonstrated that the value of γ decreases from to 0.37 ± 0.1 to 0.35 ± 0.1 with increasing the Co from 0 at. % to 10 at. % [42–44]. In order to simultaneously improve the GFA of CuZr-based alloys and keep the high thermal stability of the B2 CuZr phase, both 10 at. % Al and 4–6 at. % Co were introduced into CuZr-based alloys. Figure 1a shows the XRD patterns of the as-cast $(Cu_{0.5}Zr_{0.5})_{90-x}Al_{10}Co_x$ (x = 4, 5, and 6 at. %) BMGs with a diameter of 2 mm. There are no crystalline reflexes in the XRD patterns but there is an obviously broad peak around $2\theta = 17.5°$, indicating that the fabricated rods are fully amorphous. Figure 1b exhibits the DSC curves measured at a heating rate of 20 K/min. With the increasing temperature, all the present alloys exhibit a similar thermal behavior with one exothermic event being preceded by a glass transition.

Accordingly, the glass transition temperature (T_g) and the onset temperature of crystallization (T_x) together with the liquidus temperature (T_L) for the investigated samples can be obtained (Table 1). Previous results have shown that the critical thickness of the fully amorphous phase for the $(Cu_{0.5}Zr_{0.5})_{90}Al_{10}$ BMGs is less than 6 mm [48], whose T_g, T_x, T_L, and γ are about 714 K, 787 K, 1230 K, and 0.406, respectively. Meanwhile, the values of γ for the $Cu_{50-x}Zr_{50}Co_x$ (x = 0, 0.5, 2, 4, 5, 7.5, 10, 15, and 20 at. %) amorphous ribbons decrease from 0.377 to 0.327 while those for the $(Cu_{0.5}Zr_{0.5})_{100-x}Co_x$ (0, 5, 12.5, 22.5, and 23 at. %) amorphous ribbons are less than 0.377 [31,33,42–44]. However, for the $(Cu_{0.5}Zr_{0.5})_{90-x}Al_{10}Co_x$ (x = 4, 5, and 6 at. %) BMGs, the values of T_g and T_x increase to 725–733 K and 782–790 K and the corresponding γ locates between 0.398 ± 0.003 and 0.399 ± 0.003, implying that the GFA of Cu-Zr-Al-Co alloys is still good. It has been proposed that the GFA of an alloy strongly depends on the stability of the supercooled liquid and the resistance to crystallization [47]. As listed in Table 1, the widths of the supercooled liquid region ($\Delta T_{rg} = T_x - T_g$) for the $(Cu_{0.5}Zr_{0.5})_{90-x}Al_{10}Co_x$ (x = 4, 5,

and 6 at. %) BMGs, which is usually used to estimate the stability of the supercooled liquid against crystallization [49], were calculated to be larger than 55 K. This means that the thermal stabilities of the supercooled liquids are higher than those of Cu-Zr-(Co) metallic glasses but lower than that of $(Cu_{0.5}Zr_{0.5})_{90}Al_{10}$ BMG (i.e., 77 ± 5 [48]). Such facts further confirm the change tendency of the GFA mentioned above. Furthermore, a high-temperature solid phase transformation (HTSPT) from low-temperature crystallization products to the B2 CuZr phase for near-equiatomic CuZr-based BMGs usually appears between the crystallization and melting events [33]. For the CuZr-based BMGs with the addition of high-content Ag or rare earth metals, such a high-temperature HTSPT shifts to high temperatures and even overlaps with melting peaks [33]. On the contrary, the addition of Co with a content higher than 4 at. % would stabilize the B2 CuZr phase into low temperatures, leading to the overlap of crystallization and such a high-temperature HTSPT [31,33,42–44]. In our case, no obvious endothermic peaks can be observed between crystallization and melting events. Therefore, the addition of Al and Co could stabilize the B2 phase to low temperatures or enhance the HTSPT temperature.
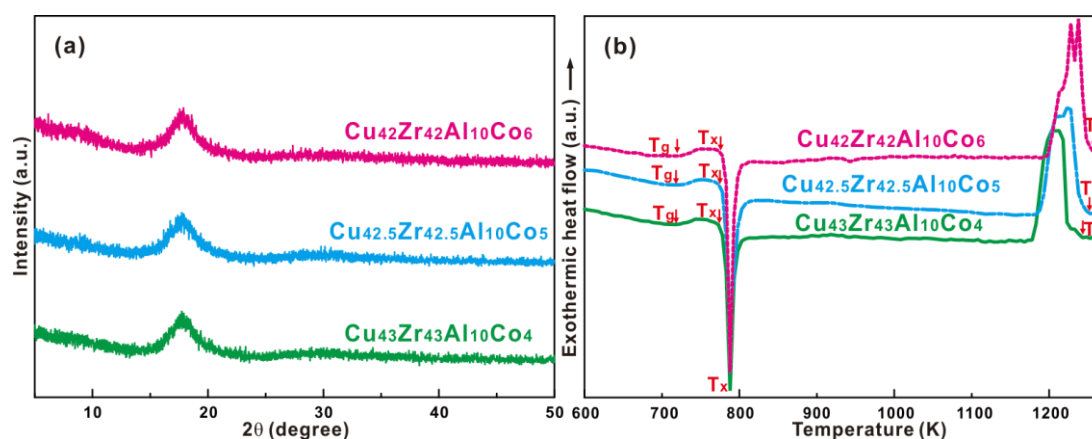

Figure 1. (**a**) XRD patterns of the $(Cu_{0.5}Zr_{0.5})_{90-x}Al_{10}Co_x$ (x = 4, 5, and 6 at. %) BMGs with a diameter of 2 mm; (**b**) DSC curves of the as-cast BMGs at a heating rate of 20 K/min.

Table 1. Thermal parameters of the as-cast $(Cu_{0.5}Zr_{0.5})_{90-x}Al_{10}Co_x$ (x = 4, 5, and 6 at. %) BMGs.

Compositions	T_g (K)	T_x (K)	ΔT_{rg}	T_L (K)	γ
$(Cu_{0.5}Zr_{0.5})_{86}Al_{10}Co_4$	725 ± 2	783 ± 2	58 ± 4	1239 ± 5	0.399 ± 0.003
$(Cu_{0.5}Zr_{0.5})_{85}Al_{10}Co_5$	726 ± 2	782 ± 2	56 ± 4	1241 ± 5	0.398 ± 0.003
$(Cu_{0.5}Zr_{0.5})_{84}Al_{10}Co_6$	733 ± 2	789 ± 2	57 ± 4	1249 ± 5	0.398 ± 0.003

3.2. Primary Precipitates from Partially Crystallized Cu-Zr-Al-Co Bulk Metallic Glasses or from Rapid Solidification

In order to clarify the effects of the Co and Al additions on the thermal stability of the B2 CuZr phase, the microstructural evolutions of the present samples annealed above the T_x were investigated. Figure 2 shows the XRD patterns of the as-annealed $(Cu_{0.5}Zr_{0.5})_{90-x}Al_{10}Co_x$ (x = 4, 5, and 6 at. %) samples. In general, for most of CuZr-based BMGs, the dominant crystallization products are $Cu_{10}Zr_7$, $CuZr_2$, and/or $AlCu_2Zr$ and others, but not B2 CuZr crystals [33]. However, the primary crystallization products for the present BMGs are the B2 CuZr phase during the early stage of the crystallization. With the gradually increasing annealing temperature, the volume fraction of the B2 CuZr crystals increases gradually together with the precipitation of some $Cu_{10}Zr_7$ and $AlCu_2Zr$ crystals (Figure 2). That implies that the B2 CuZr phase is indeed stabilized to low temperatures but not the HTSPT temperature is enhanced. The enhanced thermal stability of the B2 CuZr phase with the addition of Co puts the B2 phase in a strong position during the competition between vitrification and crystallization during quenching, leading to the deterioration of the GFA to some degree. Furthermore, a small

percentage of Al in Cu-Zr-Al alloys has been proven to dramatically enhance the population of full icosahedra and their connectivity [50]. In addition, ab initio calculations also showed that the electronic interactions involving the Al addition are bond-specific and environment-specific. As a result, the associated bond shortening can strongly affect the type, frequency, and stability of the coordination polyhedral [50]. Overall, the present Cu-Zr-Al-Co alloy systems still can maintain a relatively good GFA.
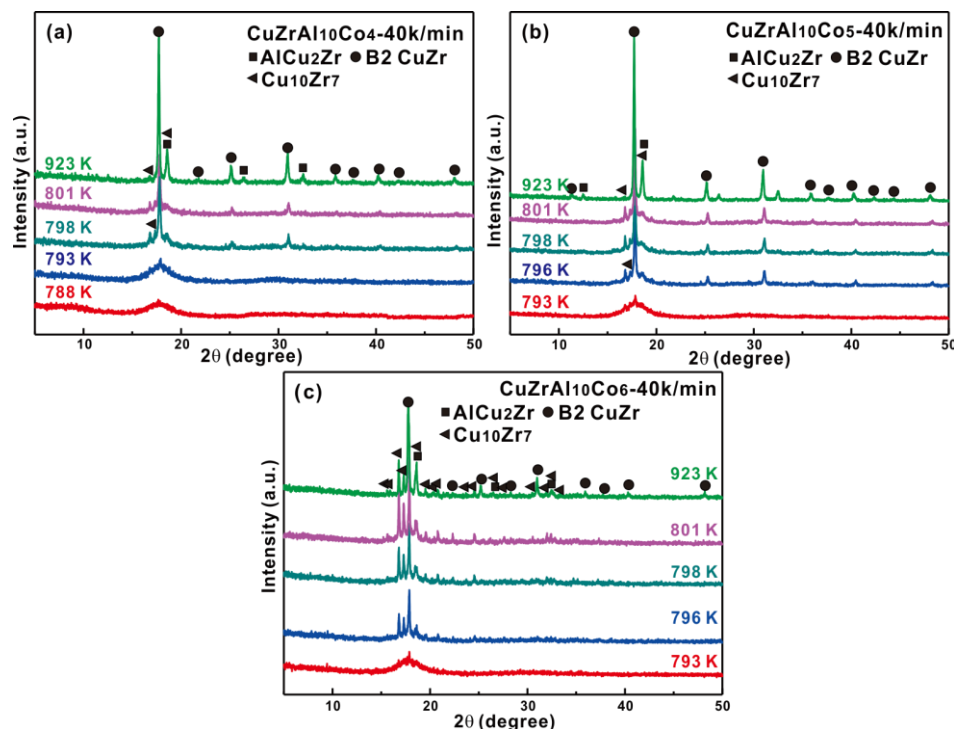

Figure 2. XRD patterns of the as-annealed $(Cu_{0.5}Zr_{0.5})_{90-x}Al_{10}Co_x$ (x = (**a**) 4; (**b**) 5; and (**c**) 6 at. %) samples at a heating rate of 40 K/min at temperatures as indexed in the present figures.

On the other hand, the primary precipitates in the glassy matrix during quenching were also investigated. A wedge-shaped sample was fabricated using an injection machine whose cooling rate is relatively lower than that of the suction casting machine in our case [51]. Hence, the critical thickness of the fully amorphous phase for the $(Cu_{0.5}Zr_{0.5})_{84}Al_{10}Co_6$ sample obtained under the current casting condition is less than 2 mm (i.e., 1.4 mm). It has been shown that the thickness of the fully amorphous phase for the as-cast samples can be used to roughly evaluate the change tendency of the applied cooling rate, i.e., the larger the dimension the sample owns, the higher the applied cooling rate becomes [52].

As shown in Figure 3 (see the yellow arrows and the inserted XRD pattern), it is clear that the B2 CuZr crystals together with a small amount of CuZr martensites, $Cu_{10}Zr_7$ and $AlCu_2Zr$ crystals precipitate in the glassy matrix. Meanwhile, with decreasing the applied cooling rate, the crystalline volume fraction gradually increases. The species of most precipitates from quenching are identical to the crystallization products upon heating Cu-Zr-Al-Co BMGs. Besides, the formation of CuZr martensites is expected to be induced by the internal stress from the quenching [29,53]. Under a high cooling rate (i.e., the thickness of the sample is less than approximately 1.8 mm), there are very few well-separated B2 crystals with an approximately spherical shape distributing in the glassy matrix (see the blue circle in Figure 3). When the volume fraction of the B2 crystals approaches 10 ± 2 vol. %, the spherical crystals trend to impinge upon each other (see the A region in Figure 3). This interpenetration process continues with increasing the crystalline volume fraction and then an obvious structural framework composed by B2 crystals starts to form at a critical volume fraction of

33 ± 2 vol. %. Such a microstructural transition can be quantified by the percolation theory [29,30]. Generally speaking, the percolation threshold for dual-phase composites locates between 10 vol. % and 50 vol. % [54], which strongly depends on the morphologies and sizes of the reinforced phase and the size ratios of the constituent phases. Pauly, Liu, and Fu et al. concluded the critical crystalline volume fraction for the microstructural transition in Cu-Zr-Al BMG composites was determined to lie between 30 and 50 vol. % [29,30,55], while it is about 35 vol. % for Zr-based BMG composites. In our case, the percolation threshold can be determined to be between 10 ± 2 vol. % and 31 ± 2 vol. % for Cu-Zr-Al-Co BMG composites.
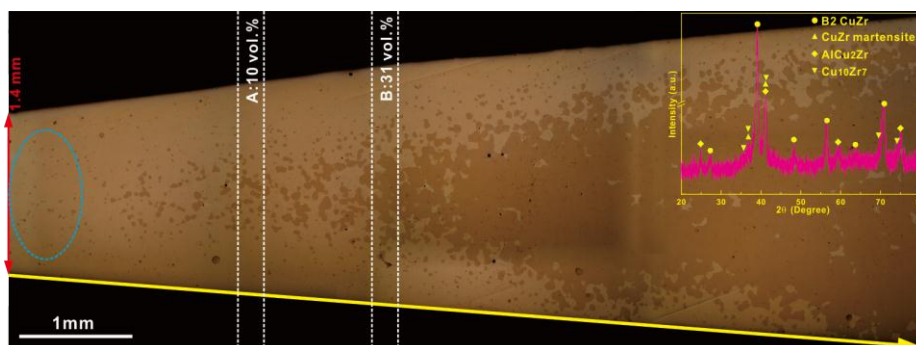

Figure 3. OM image of the as-quenched $(Cu_{0.5}Zr_{0.5})_{84}Al_{10}Co_6$ BMG composites with a wedge-shape.

3.3. Crytallization Kinetics of Cu-Zr-Al-Co Bulk Metallic Glasses

Since kinetic effects can also play an important role in the formation of BMGs during the solidification of metallic glass-forming liquids [47], the crystallization kinetics of the B2 CuZr phase in Cu-Zr-Al-Co BMGs were investigated. It has been shown that the apparent activation energies of crystallization were calculated based on the dependences of T_x and T_p on heating rates according to the Ozawa method and Kissinger equation, respectively [56–58]:

$$\ln(\varphi) = A - E_x/RT \tag{1}$$

$$\ln(\varphi/T^2) = B - E_p/RT \tag{2}$$

where φ is the heating rate, R is the gas constant, T is the characteristic temperature, and A and B are the constant. E_x and E_p are the apparent activation energies of crystallization at T_x and T_p, respectively.

As shown in Figure 4a, the isochronal DSC measurements at different heating rates for $(Cu_{0.5}Zr_{0.5})_{90-x}Al_{10}Co_x$ (x = 4, 5, and 6 at. %) samples were conducted (for clarity only selected results). With increasing Co in Cu-Zr-Al MGs, the value of E_x increases first from 386 ± 30 kJ/mol to 486 ± 26 kJ/mol and then decreases to 395 ± 15 kJ (Figure 4b–d). Meanwhile, the value of E_p increases gradually from 320 ± 16 kJ/mol to 400 ± 25 kJ/mol, respectively (Figure 4b–d). Such observations show that the resistance to crystallization is enhanced with the addition of Co into Cu-Zr-Al MGs. Since Co can be easily dissolved into the B2 CuZr phase and other crystalline precipitates [34–36] and then enhance the thermal stability of the B2 CuZr phase, the driving force for the precipitates in the glassy matrix could be enhanced, leading to the increases of E_x and E_p. Furthermore, the E_x being larger than E_p for each alloy also implies the crystallization products, i.e., B2 CuZr crystals together with a little $Cu_{10}Zr_7$ and $AlCu_2Zr$, require less activation energy to grow up after the nucleation of B2 CuZr crystals.
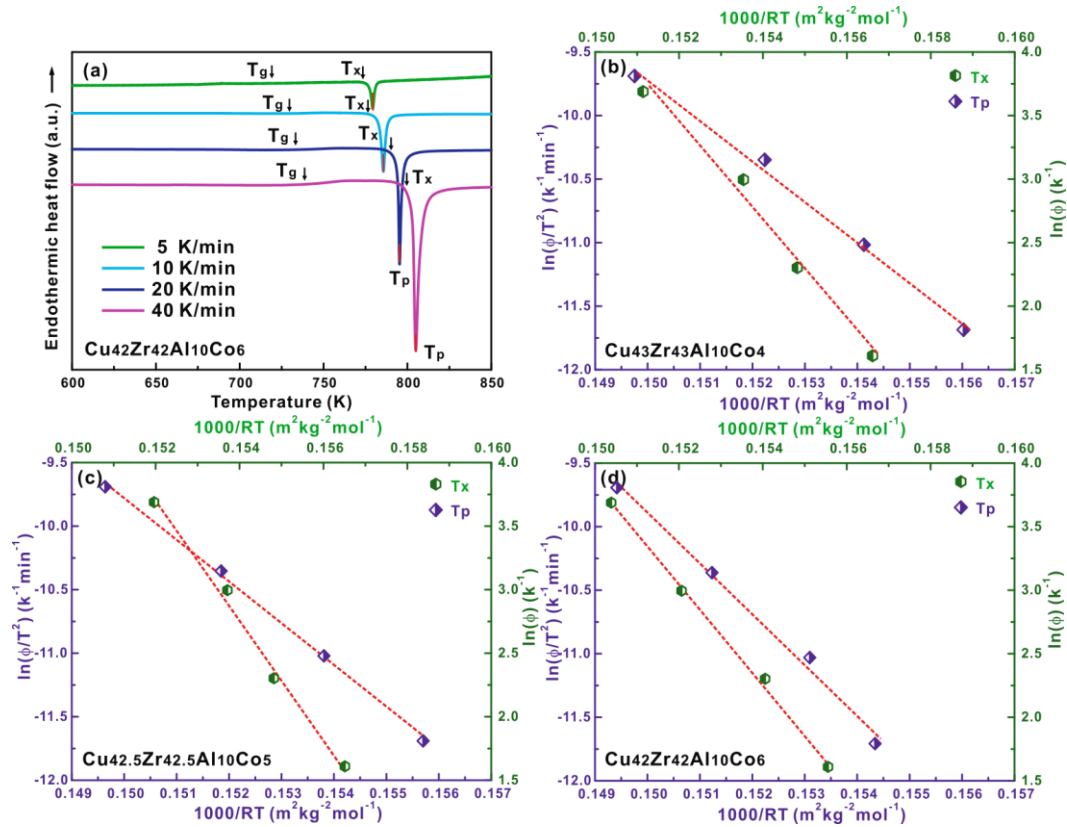
Figure 4. (**a**) DSC curves for the $(Cu_{0.5}Zr_{0.5})_{84}Al_{10}Co_6$ BMGs at different heating rates, and the Ozawa and Kissinger plots based on the isochronal DSC measurements for $(Cu_{0.5}Zr_{0.5})_{90-x}Al_{10}Co_x$ (x = (**b**) 4, (**c**) 5, and (**d**) 6 at. %) samples.

In order to further clarify the nucleation and growth mechanisms of the B2 CuZr phase during the early stage of crystallization, the Johnson-Mehl-Avrami (JMA) analysis was conducted based on the isothermal curves for $(Cu_{50}Zr_{50})_{84}Al_{10}Co_6$ BMGs at different temperatures (Figure 5). Meanwhile, the corresponding crystalline volume fraction (x) was calculated as a function of the annealing time and temperature (see the inset in Figure 5). In an attempt to describe the isothermal phase transformation for the investigated samples, the JMA model was adopted [59–61]:

$$x(t) = 1 - \exp\{-[K(t - \tau)]^n\} \tag{3}$$

where $x(t)$ is the crystalline volume fraction at different annealing time (t), τ is the incubation time, and n is the Avrami exponent correlated with the nucleation and growth mechanisms. Then the value of K is determined by [59–61]:

$$K = K_0 \cdot \exp(-E_a/RT) \tag{4}$$

As shown in Figure 5b,c, with increasing the annealing temperature from 793 K to 798 K, the volume fraction of precipitates is enhanced from about 1 vol. % to 12 vol. %. Meanwhile, it is worth noting that some spherical crystals uniformly distribute in the glassy matrix and their corresponding size increases from 1.75 ± 0.75 μm to 4.5 ± 3 μm with the increasing crystalline volume fraction. Furthermore, the amount of the nucleation sites almost stays constant but only the sizes of the spherical precipitates become larger. The EDX measurements (Figure 6) show that the concentration of B2 CuZr precipitates (i.e., $Cu_{37.4}Zr_{46.2}Al_{9.7}Co_{6.7}$) is almost identical to that of the remaining glassy matrix (i.e., $Cu_{38.8}Zr_{45.2}Al_{9.2}Co_{6.8}$). Furthermore, previous reports have shown that the formation of the B2 CuZr phase is polymorphic [29]. All these facts imply that the growth of the B2 CuZr phase during the

early crystallization is interface-controlled, being the same as the crystallization of Cu-Zr-Al/Ag/Ti BMGs [38,46,62,63] but different from the diffusion-controlled crystallization of Cu-Zr-Al-Ag/Y/Ni BMGs [64–66].
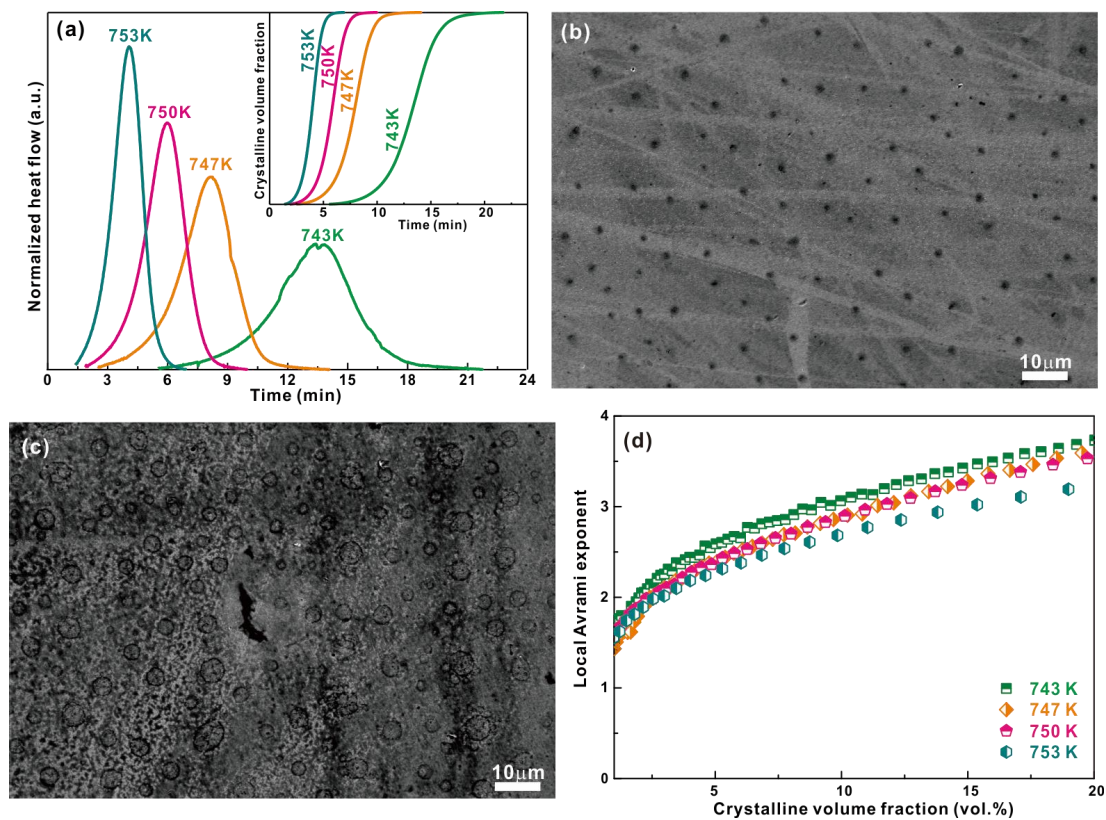

Figure 5. (**a**) Isothermal DSC curves as a function of annealing time for the $(Cu_{0.5}Zr_{0.5})_{84}Al_{10}Co_6$ BMGs and the corresponding crystalline volume fractions (see the inset); SEM images of the as-annealed $(Cu_{0.5}Zr_{0.5})_{84}Al_{10}Co_6$ samples at a heating rate of 40 K/min at 793 K (**b**) and 798 K (**c**), respectively, and (**d**) the Avrami exponents as a function of the crystalline volume fractions.
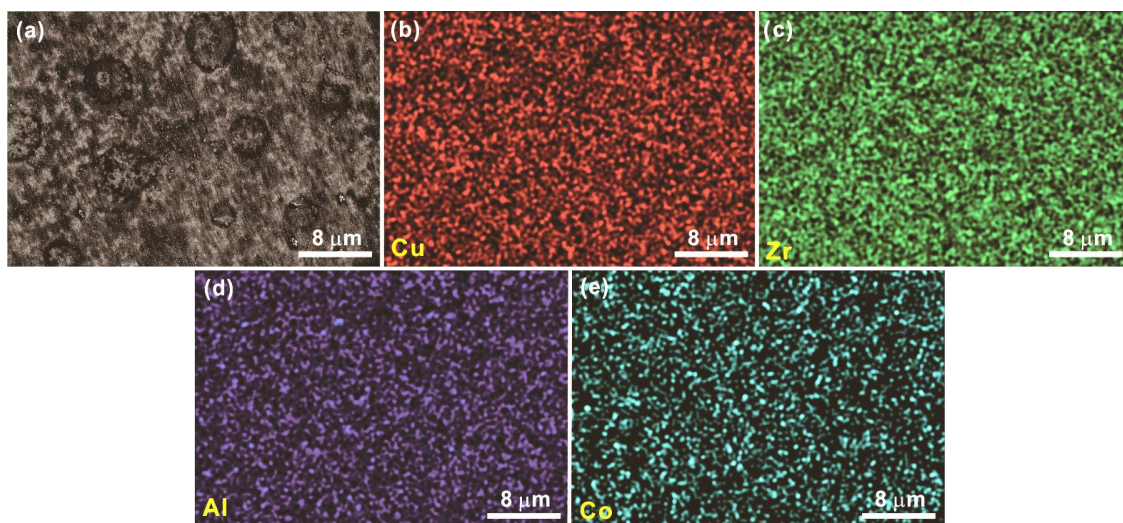

Figure 6. (**a**) Amplificatory SEM images of the as-annealed $(Cu_{0.5}Zr_{0.5})_{84}Al_{10}Co_6$ samples at a heating rate of 40 K/min at 793 K, and the EDX results for the elements (**b**) Cu, (**c**) Zr, (**d**) Al, and (**e**) Co in the present samples.

Since the early crystallization is mainly dominated by the formation of B2 CuZr crystals and the subsequent crystallization is governed by the B2 CuZr crystals and other crystals, here the local Avrami exponents (*n*) were calculated from the slope of the fitting curves of $\ln\{\ln[1/(1-x)]\}$ vs. $\ln(t-\tau)$ when the crystalline volume fraction (*x*) locates between 1 vol. % and 20 vol. % (Figure 5d). When the *x*-value lies between 1 vol. % and 20 vol. %, the local Avrami exponents (*n*) for the investigated samples gradually increase from about 1.75 to 3.5. It has been shown [58,67] that the Avrami exponent can be determined by a linear relationship, $n = a + bp$, where *a* is a nucleation parameter, *b* represents the dimensionality of the crystal growth, and *p* is the growth index. In our case, with no need for long-range diffusion, polymorphic B2 crystal growth rates are often fast and isotropic even though the simultaneous formation of crystalline precipitates from the parent amorphous phase requires diffusion at or near to the transformation front [68], leading to a constant *p* of 1 throughout the early crystallization. In the beginning, the crystallization of the present BMGs without any change in concentration into a stable crystalline compound can be observed and the nucleation of the precipitates becomes more active. Then a rapid increase of the nucleation rate of the B2 CuZr phase can be induced before the *x*-value reaches 1 vol. %. When the *n* exponent gradually increases up to 3, the nucleation rate is gradually close to zero and then the crystalline volume fraction is mainly controlled by the growth of the pre-existing B2 CuZr precipitate. That corresponds well with our SEM measurements. Therefore, the value of *b* during the early crystallization roughly increases from 2 to 3. Therefore, the early crystallization of the present BMGs should be interface-controlled two- and three-dimensional growth at almost a zero nucleation rate. Afterwards, other stable crystalline compounds, i.e., $AlCu_2Zr$ and $Cu_{10}Zr_7$, start to precipitate in the glassy matrix, resulting in the further increase of the *n* exponent. Such observations implying that it should be easy to control the partial crystallization of Cu-Zr-Al-Co BMGs, which is helpful to control the formation of the B2 CuZr phase using the fast and partial crystallization method [33].

4. Conclusions

In this study, novel $(Cu_{0.5}Zr_{0.5})_{90-x}Al_{10}Co_x$ (*x* = 4, 5, and 6 at. %) BMGs with good GFA and high thermal stability were prepared. With the addition of Co and Al into CuZr-based alloys, the width of the supercooled liquid is relatively larger than the Cu-Zr-Co amorphous ribbons but smaller than the Cu-Zr-Al BMG, while the activation energies of crystallization exceed 300 kJ/mol. Furthermore, the dominant crystallization products upon heating the present BMGs are identical to the precipitates from Cu-Zr-Al-Co melts during quenching, i.e., the B2 CuZr crystals. Furthermore, during quenching, the spherical crystals trend to impinge upon each other when the volume fraction of B2 crystals approaches 10 ± 2 vol. % and this interpenetration process continues at a critical volume fraction of 33 ± 2 vol. %. Studies on the early crystallization kinetics of the present BMGs show that the nucleation and growth is interface-controlled two- and three-dimensional growth. The fabricated BMGs could be a good candidate to fabricate ductile BMG composites by controlling rapid solidification or by rapidly and partially crystallizing BMGs.

Author Contributions: K.S. and L.W. conceived and designed the experiments; X.H., Y.Q., K.Q., and K.S. performed experiments; K.S., L.W., X.H., and Y.S. analyzed the data; X.L., S.H., and J.M. contributed reagents/materials/analysis tools; K.S. and L.W. wrote the paper.

Conflicts of Interest: The authors declare no conflict of interest.

References

1. Huang, L.J.; Geng, L.; Peng, H.X. Microstructurally inhomogeneous composites: Is a homogeneous reinforcement distribution optimal? *Prog. Mater. Sci.* **2015**, *71*, 93–168. [CrossRef]

2. Ritchie, R.O. The conflicts between strength and toughness. *Nat. Mater.* **2011**, *10*, 817–822. [CrossRef] [PubMed]

3. Casati, R.; Vedani, M. Metal matrix composites reinforced by nano-particles—A review. *Metals* **2014**, *4*, 65. [CrossRef]

4. Wong, P.; Lee, T.; Tsai, P.; Cheng, C.; Li, C.; Jang, J.; Huang, J. Enhanced mechanical properties of MgZnCa bulk metallic glass composites with Ti-particle dispersion. *Metals* **2016**, *6*, 116. [CrossRef]

5. Madge, S.; Louzguine-Luzgin, D.; Inoue, A.; Greer, A. Large compressive plasticity in a La-based glass-crystal composite. *Metals* **2013**, *3*, 41. [CrossRef]

6. Chang, H.J.; Yook, W.; Park, E.S.; Kyeong, J.S.; Kim, D.H. Synthesis of metallic glass composites using phase separation phenomena. *Acta Mater.* **2010**, *58*, 2483–2491. [CrossRef]

7. Choi-Yim, H.; Conner, R.D.; Szuecs, F.; Johnson, W.L. Processing, microstructure and properties of ductile metal particulate reinforced $Zr_{57}Nb_5Al_{10}Cu_{15.4}Ni_{12.6}$ bulk metallic glass composites. *Acta Mater.* **2002**, *50*, 2737–2745. [CrossRef]

8. Eckert, J.; Das, J.; Pauly, S.; Duhamel, C. Processing routes, microstructure and mechanical properties of metallic glasses and their composites. *Adv. Eng. Mater.* **2007**, *9*, 443–453. [CrossRef]

9. Fan, C.; Inoue, A. Ductility of bulk nanocrystalline composites and metallic glasses at room temperature. *Appl. Phys. Lett.* **2000**, *77*, 46–48. [CrossRef]

10. Pan, D.G.; Zhang, H.F.; Wang, A.M.; Hu, Z.Q. Enhanced plasticity in Mg-based bulk metallic glass composite reinforced with ductile Nb particles. *Appl. Phys. Lett.* **2006**, *89*, 261904. [CrossRef]

11. Li, Y.; Poon, S.J.; Shiflet, G.J.; Xu, J.; Kim, D.H.; Loffler, J.F. Formation of bulk metallic glasses and their composites. *MRS Bull.* **2007**, *32*, 624–628. [CrossRef]

12. Hofmann, D.C.; Suh, J.Y.; Wiest, A.; Duan, G.; Lind, M.L.; Demetriou, M.D.; Johnson, W.L. Designing metallic glass matrix composites with high toughness and tensile ductility. *Nature* **2008**, *451*, 1085–1089. [CrossRef] [PubMed]

13. Choi-Yim, H.; Conner, R.D.; Szuecs, F.; Johnson, W.L. Quasistatic and dynamic deformation of tungsten reinforced $Zr_{57}Nb_5Al_{10}Cu_{15.4}Ni_{12.6}$ bulk metallic glass matrix composites. *Scr. Mater.* **2001**, *45*, 1039–1045. [CrossRef]

14. Fu, H.M.; Wang, H.; Zhang, H.F.; Hu, Z.Q. In situ TiB-reinforced cu-based bulk metallic glass composites. *Scr. Mater.* **2006**, *54*, 1961–1966. [CrossRef]

15. Guo, S.F.; Liu, L.; Li, N.; Li, Y. Fe-based bulk metallic glass matrix composite with large plasticity. *Scr. Mater.* **2010**, *62*, 329–332. [CrossRef]

16. Qiao, J.W.; Sun, A.C.; Huang, E.W.; Zhang, Y.; Liaw, P.K.; Chuang, C.P. Tensile deformation micromechanisms for bulk metallic glass matrix composites: From work-hardening to softening. *Acta Mater.* **2011**, *59*, 4126–4137. [CrossRef]

17. Abdeljawad, F.; Haataja, M. Continuum modeling of bulk metallic glasses and composites. *Phys. Rev. Lett.* **2010**, *105*, 125503. [CrossRef] [PubMed]

18. Hays, C.C.; Kim, C.P.; Johnson, W.L. Microstructure controlled shear band pattern formation and enhanced plasticity of bulk metallic glasses containing in situ formed ductile phase dendrite dispersions. *Phys. Rev. Lett.* **2000**, *84*, 2901–2904. [CrossRef] [PubMed]

19. Qiao, J.W.; Zhang, T.; Yang, F.Q.; Liaw, P.K.; Pauly, S.; Xu, B.S. A tensile deformation model for in-situ dendrite/metallic glass matrix composites. *Sci. Rep.* **2013**, *3*, 2816. [CrossRef] [PubMed]

20. Wu, F.F.; Chan, K.C.; Jiang, S.S.; Chen, S.H.; Wang, G. Bulk metallic glass composite with good tensile ductility, high strength and large elastic strain limit. *Sci. Rep.* **2014**, *4*, 5302. [CrossRef] [PubMed]

21. Liu, Z.Q.; Liu, G.; Qu, R.T.; Zhang, Z.F.; Wu, S.J.; Zhang, T. Microstructural percolation assisted breakthrough of trade-off between strength and ductility in CuZr-based metallic glass composites. *Sci. Rep.* **2014**, *4*, 4167. [CrossRef] [PubMed]

22. Hofmann, D.C. Shape memory bulk metallic glass composites. *Science* **2010**, *329*, 1294–1295. [CrossRef] [PubMed]

23. Wu, D.; Song, K.; Cao, C.; Li, R.; Wang, G.; Wu, Y.; Wan, F.; Ding, F.; Shi, Y.; Bai, X.; et al. Deformation-induced martensitic transformation in Cu-Zr-Zn bulk metallic glass composites. *Metals* **2015**, *5*, 2134. [CrossRef]

24. Song, K.K.; Pauly, S.; Zhang, Y.; Sun, B.A.; He, J.; Ma, G.Z.; Kuhn, U.; Eckert, J. Thermal stability and mechanical properties of $Cu_{46}Zr_{46}Ag_8$ bulk metallic glass and its composites. *Mater. Sci. Eng. A* **2013**, *559*, 711–718. [CrossRef]

25. Xie, M.T.; Zhang, P.N.; Song, K.K. Thermal stability and transformation-mediated deformability of Cu-Zr-Al-Ni bulk metallic glass composite. *J. Mater. Sci. Technol.* **2013**, *29*, 868–872. [CrossRef]

26. Song, K.K.; Pauly, S.; Sun, B.A.; Zhang, Y.; Tan, J.; Kühn, U.; Stoica, M.; Eckert, J. Formation of Cu-Zr-Al-Er bulk metallic glass composites with enhanced deformability. *Intermetallics* **2012**, *30*, 132–138. [CrossRef]

27. Song, K.K.; Pauly, S.; Sun, B.A.; Tan, J.; Stoica, M.; Kuhn, U.; Eckert, J. Correlation between the microstructures and the deformation mechanisms of CuZr-based bulk metallic glass composites. *AIP Adv.* **2013**, *3*, 012116. [CrossRef]

28. Wu, Y.; Xiao, Y.; Chen, G.; Liu, C.T.; Lu, Z. Bulk metallic glass composites with transformation-mediated work-hardening and ductility. *Adv. Mater.* **2010**, *22*, 2770–2773. [CrossRef] [PubMed]

29. Pauly, S.; Liu, G.; Wang, G.; Kuhn, U.; Mattern, N.; Eckert, J. Microstructural heterogeneities governing the deformation of $Cu_{47.5}Zr_{47.5}Al_5$ bulk metallic glass composites. *Acta Mater.* **2009**, *57*, 5445–5453. [CrossRef]

30. Liu, Z.Q.; Li, R.; Liu, G.; Su, W.H.; Wang, H.; Li, Y.; Shi, M.J.; Luo, X.K.; Wu, G.J.; Zhang, T. Microstructural tailoring and improvement of mechanical properties in CuZr-based bulk metallic glass composites. *Acta Mater.* **2012**, *60*, 3128–3139. [CrossRef]

31. Wu, Y.; Wang, H.; Wu, H.H.; Zhang, Z.Y.; Hui, X.D.; Chen, G.L.; Ma, D.; Wang, X.L.; Lu, Z.P. Formation of Cu-Zr-Al bulk metallic glass composites with improved tensile properties. *Acta Mater.* **2011**, *59*, 2928–2936. [CrossRef]

32. Liu, Z.Q.; Li, R.; Liu, G.; Song, K.K.; Pauly, S.; Zhang, T.; Eckert, J. Pronounced ductility in CuZrAl ternary bulk metallic glass composites with optimized microstructure through melt adjustment. *AIP Adv.* **2012**, *2*, 032176. [CrossRef]

33. Song, K.K.; Pauly, S.; Zhang, Y.; Gargarella, P.; Li, R.; Barekar, N.S.; Kühn, U.; Stoica, M.; Eckert, J. Strategy for pinpointing the formation of B2 CuZr in metastable CuZr-based shape memory alloys. *Acta Mater.* **2011**, *59*, 6620–6630. [CrossRef]

34. Javid, F.A.; Mattern, N.; Pauly, S.; Eckert, J. Effect of cobalt on phase formation, microstructure, and mechanical properties of $Cu_{50-x}Co_xZr_{50}$ (x = 2, 5, 10, 20 at. pct) alloys. *Metall. Mater. Trans. A* **2012**, *43A*, 2631–2636. [CrossRef]

35. Javid, F.A.; Mattern, N.; Khoshkhoo, M.S.; Stoica, M.; Pauly, S.; Eckert, J. Phase formation of $Cu_{50-x}Co_xZr_{50}$ (x = 0–20 at. %) alloys: Influence of cooling rate. *J. Alloy. Compd.* **2014**, *590*, 428–434. [CrossRef]

36. Kosiba, K.; Gargarella, P.; Pauly, S.; Kuhn, U.; Eckert, J. Predicted glass-forming ability of Cu-Zr-Co alloys and their crystallization behavior. *J. Appl. Phys.* **2013**, *113*, 123505. [CrossRef]

37. Pauly, S.; Das, J.; Bednarcik, J.; Mattern, N.; Kim, K.B.; Kim, D.H.; Eckert, J. Deformation-induced martensitic transformation in Cu-Zr-(Al,Ti) bulk metallic glass composites. *Scr. Mater.* **2009**, *60*, 431–434. [CrossRef]

38. Song, K.K.; Gargarella, P.; Pauly, S.; Ma, G.Z.; Kuhn, U.; Eckert, J. Correlation between glass-forming ability, thermal stability, and crystallization kinetics of Cu-Zr-Ag metallic glasses. *J. Appl. Phys.* **2012**, *112*, 063503. [CrossRef]

39. Fu, J.; Men, H.; Pang, S.; Ma, C.; Zhang, T. Formation and thermal stability of Cu-Zr-Al-Er bulk metallic glasses with high glass-forming ability. *J. Univ. Sci. Technol. B.* **2007**, *14*, 36–38. [CrossRef]

40. Fan, G.J.; Li, J.J.Z.; Rhim, W.-K.; Qiao, D.C.; Choo, H.; Liaw, P.K.; Johnson, W.L. Thermophysical properties of a $Cu_{46}Zr_{42}Al_7Y_5$ bulk metallic glass-forming liquid. *Appl. Phys. Lett.* **2006**, *88*, 221909. [CrossRef]

41. Duan, G.; de Blauwe, K.; Lind, M.L.; Schramm, J.P.; Johnson, W.L. Compositional dependence of thermal, elastic, and mechanical properties in Cu-Zr-Ag bulk metallic glasses. *Scr. Mater.* **2008**, *58*, 159–162. [CrossRef]

42. Kuo, C.N.; Huang, J.C.; Du, X.H.; Liu, X.J.; Nieh, T.G. Comparison of mechanical response in CuZrAl-V and CuZrAl-Co bulk metallic glass composites. *J. Alloy. Compd.* **2014**, *586*, S14–S19. [CrossRef]

43. Gao, W.H.; Meng, X.L.; Cai, W.; Zhao, L.C. Effects of Co and Al addition on martensitic transformation and microstructure in ZrCu-based shape memory alloys. *Trans. Nonferr. Met. Soc. China* **2015**, *25*, 850–855. [CrossRef]

44. Wei, Y.; Du, J.; Chen, R. Martensitic transformation induced plasticity in ZrCuAl metallic glass composites: Precipitate size and volume effects. *Intermetallics* **2016**, *68*, 1–4. [CrossRef]

45. Okulov, I.V.; Soldatov, I.V.; Sarmanova, M.F.; Kaban, I.; Gemming, T.; Edstrom, K.; Eckert, J. Flash joule heating for ductilization of metallic glasses. *Nat. Commun.* **2015**, *6*, 7932. [CrossRef] [PubMed]

46. Song, K.K. Synthesis, microstructure, and deformation mechanisms of CuZr-based bulk metallic glass composites. Ph.D. Thesis, TU Dresden, Dresden, Germany, November 2013.

47. Lu, Z.P.; Liu, C.T. A new glass-forming ability criterion for bulk metallic glasses. *Acta Mater.* **2002**, *50*, 3501–3512. [CrossRef]

48. Zhang, Q.; Zhang, W.; Xie, G.Q.; Inoue, A. Glass-forming ability and mechanical properties of the ternary Cu-Zr-Al and quaternary Cu-Zr-Al-Ag bulk metallic glasses. *Mater. Trans.* **2007**, *48*, 1626–1630. [CrossRef]

49. Inoue, A. Stabilization of metallic supercooled liquid and bulk amorphous alloys. *Acta Mater.* **2000**, *48*, 279–306. [CrossRef]

50. Cheng, Y.Q.; Ma, E.; Sheng, H.W. Atomic level structure in multicomponent bulk metallic glass. *Phys. Rev. Lett.* **2009**, *102*, 245501. [CrossRef] [PubMed]

51. Song, K.K.; Pauly, S.; Zhang, Y.; Li, R.; Gorantla, S.; Narayanan, N.; Kuhn, U.; Gemming, T.; Eckert, J. Triple yielding and deformation mechanisms in metastable $Cu_{47.5}Zr_{47.5}Al_5$ composites. *Acta Mater.* **2012**, *60*, 6000–6012. [CrossRef]

52. Srivastava, R.M.; Eckert, J.; Löser, W.; Dhindaw, B.K.; Schultz, L. Cooling rate evaluation for bulk amorphous alloys from eutectic microstructures in casting processes. *Mater. Trans.* **2002**, *43*, 1670–1675. [CrossRef]

53. Ju, D.Y.; Zhang, W.M.; Zhang, Y. Modeling and experimental verification of martensitic transformation plastic behavior in carbon steel for quenching process. *Mater. Sci. Eng. A* **2006**, *438–440*, 246–250. [CrossRef]

54. Nan, C.W. Physics of inhomogeneous inorganic materials. *Prog. Mater. Sci.* **1993**, *37*, 1–116. [CrossRef]

55. Fu, X.L.; Li, Y.; Schuh, C.A. Mechanical properties of metallic glass matrix composites: Effects of reinforcement character and connectivity. *Scr. Mater.* **2007**, *56*, 617–620. [CrossRef]

56. Ozawa, T. Kinetic analysis of derivative curves in thermal analysis. *J. therm. Anal. Calorim.* **1970**, *2*, 301–324. [CrossRef]

57. Kissinger, H.E. Reaction kinetics in differential thermal analysis. *Anal. Chem.* **1957**, *29*, 1702–1706. [CrossRef]

58. Andreeta, M.R.B. *Crystallization: Science and Technology*, 1st ed.; Intech: Rijeka, Croatia, 2012.

59. Avrami, M. Kinetics of phase change. I general theory. *J. Chem. Phys.* **1939**, *7*, 1103–1112. [CrossRef]

60. Avrami, M. Kinetics of phase change. II transformation-time relations for random distribution of nuclei. *J. Chem. Phys.* **1940**, *8*, 212–224. [CrossRef]

61. Johnson, W.A.; Mehl, R.F. Reaction kinetics in processes of nucleation and growth. *Trans. Am. Inst. Min. Metall. Pet. Eng.* **1939**, *135*, 416–442.

62. Pauly, S.; Das, J.; Mattern, N.; Kim, D.H.; Eckert, J. Phase formation and thermal stability in Cu-Zr-Ti(Al) metallic glasses. *Intermetallics* **2009**, *17*, 453–462. [CrossRef]

63. Xie, G.; Louzguine-Luzgin, D.V.; Zhang, Q.; Zhang, W.; Inoue, A. Structure and crystallization kinetics of a $Cu_{50}Zr_{45}Ti_5$ glassy alloy. *J. Alloy. Compd.* **2009**, *483*, 24–27. [CrossRef]

64. Qiao, J.C.; Pelletier, J.M. Crystallization kinetics in $Cu_{46}Zr_{45}Al_7Y_2$ bulk metallic glass by differential scanning calorimetry (DSC). *J. Non Cryst. Solids* **2011**, *357*, 2590–2594. [CrossRef]

65. Zhang, J.; Wei, Y.H.; Qiu, K.Q.; Zhang, H.F.; Quan, M.X.; Hu, Z.Q. Crystallization kinetics and pressure effect on crystallization of $Zr_{55}Al_{10}Ni_5Cu_{30}$ bulk metallic glass. *Mater. Sci. Eng. A* **2003**, *357*, 386–391. [CrossRef]

66. Park, S.O.; Lee, J.C.; Kim, Y.C.; Fleury, E.; Sung, D.S.; Kim, D.H. Crystallization kinetics of the $Cu_{43}Zr_{43}Al_7Ag_7$ amorphous alloy. *Mater. Sci. Eng. A* **2007**, *449–451*, 561–564. [CrossRef]

67. Christian, J.W. *The Theory of Transformation in Metals and Alloys*, 1st ed.; Pergamon Press: Oxford, UK, 1965.

68. Martin, J.W.; Doherty, R.D.; Cantor, B. *Stability of Microstructure in Metallic Systems*, 2nd ed.; Cambridge University Press: Cambridge, UK, 1997.